RESEARCH ARTICLE | MARCH 16 2018

Enhanced electron emission from coated metal targets: Effect of surface thickness on performance

Saibabu Madas; S. K. Mishra; Mousumi Upadhyay Kahaly

AIP Advances 8, 035019 (2018)
https://doi.org/10.1063/1.5012861

Enhanced electron emission from coated metal targets: Effect of surface thickness on performance

Saibabu Madas, S. K. Mishra, and Mousumi Upadhyay Kahaly[a]
Extreme Light Infrastructure-Attosecond Light Pulse Source (ELI-ALPS), Szeged, Hungary, 6720

(Received 8 November 2017; accepted 11 January 2018; published online 16 March 2018)

In this work, we establish an analytical formalism to address the temperature dependent electron emission from a metallic target with thin coating, operating at a finite temperature. Taking into account three dimensional parabolic energy dispersion for the target (base) material and suitable thickness dependent energy dispersion for the coating layer, Fermi Dirac statistics of electron energy distribution and Fowler's mechanism of the electron emission, we discuss the dependence of the emission flux on the physical properties such as the Fermi level, work function, thickness of the coating material, and operating temperature. Our systematic estimation of how the thickness of coating affects the emission current demonstrates superior emission characteristics for thin coating layer at high temperature (above 1000 K), whereas in low temperature regime, a better response is expected from thicker coating layer. This underlying fundamental behavior appears to be essentially identical for all configurations when work function of the coating layer is lower than that of the bulk target work function. The analysis and predictions could be useful in designing new coated materials with suitable thickness for applications in the field of thin film devices and field emitters. https://doi.org/10.1063/1.5012861

I. INTRODUCTION

Emission of electrons from a material is a typical consequence of the escape of the carriers from ionic potential induced surface barrier, and can be utilized in multiple applications, such as, in construction of bright electron sources for high resolution electron microscope.[1] Efficient electron emission from a material demands certain important properties, such as, good mechanical, chemical stability,[2] surface morphology,[3] and high electron emission probabilities.[4] In this context, cladding on a metal surface plays an effective role, especially for practical use, commercialization, and efficient installation in devices. Different methods for surface treatment of films are thus gaining significant attention of materials engineering community as a feasible route to further improve a target's emission properties. Surface engineering methods[5,6] such as ion-beam bombarding, hydrogen etching, metal coating, etc., are fast developing towards improved properties and performance.

In improving the electronic properties of surfaces, a general established way is to modify the effective barrier height (viz. work function) by various means of surface engineering in order to elevate the emission flux. Electronic structures and effective work functions can be engineered through effect of substrate,[7] doping,[8] or defects.[9] In a recent study,[10] a monolayer of alkali metal such as Cesium combined with appropriate proportion of oxygen is deposited on graphene to lower the work function of the material. According to this study, work function may further be reduced by electrostatic grating achieved through suitable doping of the parent material and thereby tuning the interlayer interaction with the coating. Such interaction at the interface between the target and the coating material depends on the effective interface thickness, which is also related to the thickness of coating material.

[a]Author's E-mail: Mousumi.UpadhyayKahaly@eli-alps.hu

However the dependence of effective flux on the coating thickness is little understood and demands a thorough investigation. Recently, it is observed that the dimensionality of the surface material plays significant role in determining characteristics effective field emission.[11] This clearly indicates that not only the parent or the coating material properties, but the coating thickness is also of significance in specifying the emission current from the surface. The coating thickness may even be of monoatomic layer (i.e. few angstroms), as illustrated in the study by Khalid et al.[12] In their work, monolayers of diamondoids, which are nanoscale diamond molecules are used to successfully enhance the field-emission properties from the metal surfaces. In this framework, herein we analyze physics describing the effect of coating on the electron emission properties of a coated target and specify an adequate parameter regime for its efficient operation.

Experimental results suggest that depending on the microstructure and surface morphology of the surface coating, field-emission stability and efficiency could be significantly improved, in comparison to the as-deposited films.[13] How the materials properties such as Fermi level, and work function of the surface coating in comparison to its inner bulk counterpart affects the overall performance of the field emitters is a question of immense interest. In this work, we present an analytical model to study electron emission from a coated surface, under the influence of a dc electric field. Furthermore, we compare the effective emission properties for varying thickness of the coating layer, in order to establish a simplistic route to enhance the field emission efficiency from such coated metal targets.

II. ANALYSIS

In this work, we analyze the transport properties of the electrons associated with the electron emission from the surfaces fabricated by the uniform coating of a low work function material on the planar bulk metal target (parent). Physically, the system is equivalent to a uniform metal or semi-conductor surface kept in contact with a bulk (inner) material. As soon as they are brought into contact, the free electron population transfers from the lower (coating layer) to higher (parent surface) work function material in order to equilibrate the respective Fermi levels at a common potential. As a consequence, a finite potential ($2V_0$) equivalent to the difference between their work functions develops across the interface region (thickness d) between two adjacent surfaces, resulting in an electric field inwards to the parent surface. Due to this potential/field structure the electrons inside the parent metal available for emission need to overcome the Schottky reduced triangular potential barrier while the electrons pertaining to outer coating surface should cover up enhanced step potential barrier for the emission. The energy diagram sketch of the system into consideration has been represented in Fig. 1; all the energy levels are measured from the vacuum level (say at zero potential). In figure 1, the Fermi level, bottom of the conduction band (barrier height) and work function is represented by the notations E_f, W, and ϕ, respectively, while the additional subscripts 'a' and 'b' infers the properties associated with parent and coating materials. The additional potential V_0 infers the rise/drop in the energy levels of parent/coating material due to the transfer of the electron population in achieving dynamic equilibrium of the Fermi levels, shown by broken blue lines in the figure. The Schottky reduced potential barrier is highlighted in the figure with a red arrow. In order to estimate the electron emission flux from the coated surfaces, using this electronic energy level description first we evaluate the coefficient of tunneling for the electron populations associated with parent target and coated surfaces, which has further been used to investigate the electron emission currents.

A. Evaluation of tunneling coefficient

To evaluate the coefficient of tunneling of the electrons from a coated surface, we analyze the energy configuration in two steps, viz. (*i*) tunneling of electrons from the inner parent material at a negative potential with a Schottky reduced triangular potential barrier, and (*ii*) effective tunneling of electrons from the coating surface, which offers an enhanced step potential barrier; a pictorial representation of both the cases has been shown in Fig. 1 The electrons occupancy in the potential structures is usually characterized by Schrödinger wave equation. The time independent Schrödinger

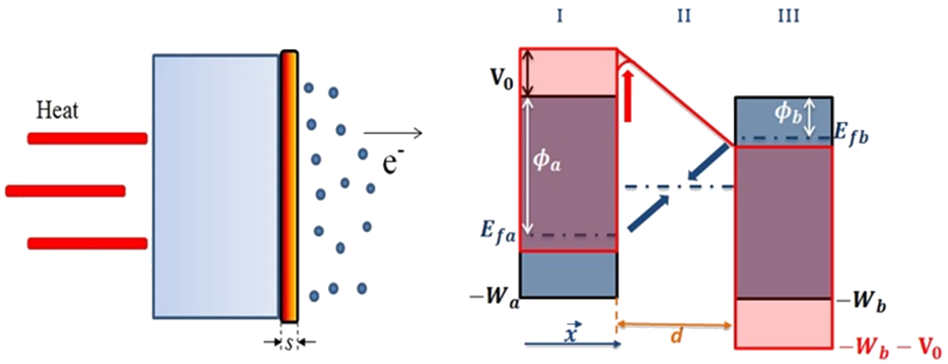

FIG. 1. Left panel refers to the heating and thermionic emission of electrons from a thin coating (width s) over metallic surface. The right hand panel corresponds to schematic diagram of energy levels of the composite system. All the energy levels are measured from the vacuum surface. Regions I, II and III corresponds to the parent target material, interface formed through coating (thickness d), and the coating materials, respectively. The blue and red color outlines refer to the energy levels in the case when the parent and coating material are kept isolated and in contact, respectively. Two blue arrows correspond to the transfer of the electron population in achieving dynamic equilibrium of the Fermi levels.

wave equation for the electrons may be written as[14,15]

$$\frac{d^2\psi}{dx^2} + \frac{2m}{\hbar^2}[E_x - V(x)]\psi = 0. \tag{1}$$

Here, E_x and $V(x)$ respectively infer the normal and potential energy of electrons in the potential structure, m refers the electronic mass and $\hbar$ is the reduced Planck's constant.

In case of the inner parent material (Fig. 1), using the respective energy structure, the potential energy $V(x)$ in three different regions may be expressed as[16–18]

$$V(x) = V_0, \qquad x < 0 \tag{2a}$$

$$V(x) = V_0(1 - 2x/d), \quad 0 \le x \le d \tag{2b}$$

and

$$V(x) = -V_0 \qquad x > d. \tag{2c}$$

Substituting the above potential energy expressions in Eq. 1, corresponding Schrödinger wave equation may be written as

$$\psi''(\varsigma) + k_1^2\psi = 0, \qquad \varsigma(= x/d) < 0 \tag{3a}$$

$$\psi''(\varsigma) + (k_2^2 + k_p^2\varsigma)\psi = 0, \quad 0 \le \varsigma \le 1 \tag{3b}$$

and

$$\psi''(\varsigma) + k_3^2\psi = 0 \qquad \varsigma > 1. \tag{3c}$$

with $\varepsilon_x = E_x/V_0, k^2 = (2mV_0d^2/\hbar^2), k_2^2 = k_1^2 = k^2(\varepsilon_x - 1), k_3^2 = k^2(\varepsilon_x + 1), k_p^2 = 2k^2$.

Considering the wave solution in these regions, the solutions of the set of Eq. 3 may be expressed as

$$\psi \equiv \psi_1 = exp(ik_1\varsigma) + b\, exp(-ik_1\varsigma), \qquad \varsigma < 0 \tag{4a}$$

$$\psi \equiv \psi_2 = c\, A_i\left[-(k_2^2 + k_p^2\varsigma)/(ik_p)^{4/3}\right] + d\, B_i\left[-(k_2^2 + k_p^2\varsigma)/(ik_p)^{4/3}\right], \quad 0 \le \varsigma \le 1 \tag{4b}$$

and

$$\psi \equiv \psi_3 = f\, exp(ik_3\varsigma) \qquad \varsigma > 1. \tag{4c}$$

In the above solutions Eq. 4a infers the incident (first term) and reflected (second term) wave in the first region ($\varsigma < 0$), while Eq. 4c corresponds to the wave transmitted to the third region ($\varsigma > 1$); the coefficients b and f infer the amplitude of the wave reflected and transmitted in first and third region.

The solution corresponding to second region infers growing (first term) and decaying (second term) waves, respectively. The transmission/reflection coefficients are calculated by using the continuity of wave function and its derivatives at the boundary layers. Using this approach and after a moderate algebra, the coefficient f referring the transmission of wave in third region may be expressed as

$$f = f_n/(f_{d1} - f_{d2}). \tag{5}$$

With

$$f_n = 2(i/k_3)(ik_p)^{2/3}\left[A_i'(c_1)B_i(c_1) - A_i(c_1)B_i'(c_1)\right]exp(-ik_3),$$
$$f_{d1} = \left[B_i(c_o) - (i/k_1)(ik_p)^{2/3}B_i'(c_o)\right]\left[A_i(c_1) + (i/k_3)(ik_p)^{2/3}A_i'(c_1)\right],$$
$$f_{d2} = \left[A_i(c_o) - (i/k_1)(ik_p)^{2/3}A_i'(c_o)\right]\left[B_i(c_1) + (i/k_3)(ik_p)^{2/3}B_i'(c_1)\right],$$
$$c_o = -k_2^2/(ik_p)^{4/3} \text{ and } c_1 = -(k_2^2 + k_p^2)/(ik_p)^{4/3}.$$

The coefficient of tunneling of the electrons to the third region can be expressed as

$$T_a = |(k_3/k_1)ff^*|, \tag{6}$$

Where f^* refers to the complex conjugate of coefficient 'f'. This expression infers the probability of the finite energy electrons reaching in the vicinity of the top layer which is an addition to the electron population in the coated surface and contributes in electron emission. Following the potential structure for the outer coated surface (Fig. 1, region III), the coefficient of tunneling corresponding to enhanced step potential barrier (by V_0) may be written as[18]

$$T_b = \frac{4\varepsilon_x^{1/2}(\varepsilon_x + w_b + 1)^{1/2}}{\left[\varepsilon_x^{1/2} + (\varepsilon_x + w_b + 1)^{1/2}\right]^{1/2}}. \tag{7}$$

where $w_b = W_b/V_0$. After a notion of the tunneling coefficient of electrons, next we evaluate the emission flux from the coated surfaces.

B. Evaluation of the emission current

Considering the bulk nature of the inner surface, the electrons in the conduction layer (Fermi sea) may be characterized by parabolic dispersion relation viz. $E = \hbar^2k^2/2m$. As obvious, image charges would build up as carriers approach the interface, resulting in slight reduction in the effective barrier height. In the presence of the induced electric field due to contact potential the effect of such "Schottky barrier" is incorporated in our analysis to raise the electron statistical distribution level to higher energy state, in the evaluation of the emission flux. Following the Fowler's treatment of the statistical distribution for the bulk metallic materials, the number of electrons hitting the surface normally (for parent surface) per unit area per unit time, having normal and parallel energy components in the range (E_x and $E_x + dE_x$) and (E_t and $E_t + dE_t$) can be expressed as[19]

$$d^2n_a = (A_o/e)T^2\left[T_a(e_x)F(e_x + e_t + \varphi_a - \upsilon_o - \upsilon_{sc})\right]de_xde_t, \tag{8}$$

where $A_o = 4\pi emk_B^2/h^3 \sim 117A/cm^2K^2$, $e_{x,t} = E_{x,t}/k_BT$, $\varphi_a = e\phi_a/k_BT$, $\upsilon_o = eV_0/k_BT$, (A_o/e) infers flux associated with Richardson constant A_o, the term $\upsilon_{sc} = (e^3\mu)^{1/2}/k_BT$ measures the lowering of the potential barrier (apparently rise in particle energy) due to Schottky effect, $\mu = 2V_0/d$ is the electric field strength. In the equation $F(E)$ corresponds to the electron energy distribution function, T refers the surface temperature and k_B is Boltzmann constant. For the present calculations, we use Fermi Dirac (FD) statistics *i.e.* $F = F_{FD} = [1 + exp(E/k_BT)]^{-1}$ for the energy distribution of electrons. The FD statistics of the electron energy distribution approaches to Maxwellian distribution (M) (*i.e.* $f \equiv f_M = exp(-E/k_BT)$) for the surfaces operating at higher temperature. After using the adequate particle distribution (say FD and M, respectively), Eq. 8 can be further simplified by integrating this over e_t space viz. $e_t \equiv (0, \infty)$ as

$$dn_{a,FD} = (A_o/e)T^2\left[T_a(e_x)\ln[1 + exp(\upsilon_o + \upsilon_{sc} - \varphi_a - e_x)\right]de_x, \tag{9a}$$

and

$$dn_{a,M} = (A_o/e)T^2\,[T_a(e_x)exp(\upsilon_o + \upsilon_{sc} - \varphi_a - e_x)]de_x. \tag{9b}$$

The expressions in Eq. 9 in fact estimates the flux of electrons that overcomes the triangular barrier at interface region, and thus enhances the electron population density for emission in addition to the pre-existing electrons at top coating layer, through enhanced step potential barrier at outer surface.

It is worth to consider the coating width, as it essentially drives the charge carrier (electron) population within the coated volume which ultimately influences the electronic transport properties. In order to evaluate the population density of electrons associated with the coating material, we use the non-parabolic thickness dependent energy dispersion relation analogous to 2D graphitic heterostructures,[20] for the electron inside the coating surface. The parallel dispersion relation for the coating top layer of thickness (s) can be expressed as[20]

$$k_t dk_t = \left(\frac{\pi\hbar}{k_B}\right)(2A_0T/e)\left(\frac{e_h^{-2a_o/s}}{(s/a_o)}\right)(E - E_x)^{(2a_o/s)-1}dE. \tag{10}$$

where $E = (E_x + E_t)$ is the total energy of the electrons inside the layer, e_h is the hopping parameter between consecutive atomic layers and a_o is the interatomic mean distance. It should be noted here that the constant term in the dispersion relation is adjusted such that the final expression of thermionic flux in the limiting case (as $s \to \infty$ i.e. bulk behaviour) is consistent with the Richardson Dushman (RD) relation. Using the above dispersion relation, the number of electrons hitting the top coated layer from inside, having total energy between E & $(E + dE)$ and normal energy between E_x & $(E_x + dE_x)$, per unit area per unit time, can be written as[21–23]

$$d^2n_b = (2A_0/e)T^2\left[e_h'^{-2a_o/s}/(s/a_o)\right](e - e_x)^{(2a_o/s)-1}F(e + \varphi_b + \upsilon_o)dede_x. \tag{11}$$

Further simplifying the above distribution by integrating over total energy (E) within range (e_x,∞), normal distribution of the electrons having FD and M statistics respectively may be rewritten as

$$dn_{b,FD} = (2A_0/e)T^2\left(\frac{e_h'^{-2a_o/s}}{(s/a_o)}\right)\Gamma(2a_o/s)\left[-Polylog\,[2a_o/s, -exp[-(e_x + \varphi_b + \upsilon_o)]]\right]de_x, \tag{12a}$$

$$dn_{b,M} = (2A_0/e)T^2\left(\frac{e_h'^{-2a_o/s}}{(s/a_o)}\right)\Gamma(2a_o/s)exp[-(e_x + \varphi_b + \upsilon_o)]de_x. \tag{12b}$$

The net normal flux of electrons available for emission from the top layer of thickness s thus may be written by adding the contributions from both viz. inner parent metal (Eq. 9) and outer surface layer population (Eq. 12) as

$$dn_{FD} = dn_{a,FD} + dn_{b,FD}, \tag{13a}$$

$$dn_M = dn_{a,M} + dn_{b,M}. \tag{13b}$$

The net electron flux coming out from the coated surface may be obtained by weighing the normal flux obtained via tunneling probability from enhanced step barrier of outer region and integrating it over adequate normal energy space *i.e.* $e_x \equiv (0,\infty)$ as

$$n_{FD} = \int_0^\infty T_b(e_x)(dn_{a,FD} + dn_{b,FD})de_x, \tag{14a}$$

and

$$n_M = \int_0^\infty T_b(e_x)(dn_{a,M} + dn_{b,M})de_x. \tag{14b}$$

It may easily be verified that in the limiting condition $s \to 0$ (i.e. without coating), using Eq. 9b along with $\upsilon_o = \upsilon_{sc} = dn_{b,M} = 0$ (corresponding to $s = 0$) and simplification $T_b = T_a = 1$, Eq. 14b reduces

to the usual Richardson Dushman law[14–19] viz. $n_M \sim (A_0/e)T^2 exp(-\varphi_a) = (A_0/e)T^2 exp(-e\phi_a/k_BT)$. The above set of equations (Eqs. 14) has numerically been examined for parametric study.

III. NUMERICAL RESULTS AND DISCUSSIONS

Based on the derivations above, in this section, we numerically analyze the effect of surface coating (viz. substrate material/width) on the electron emission flux (viz. current) from the coated surfaces operating at finite temperature. For the numerical appreciation of the analysis and illustration purpose of the conceptual basis, silver (Ag, ϕ_{Ag} = 4.5 V, W_{Ag} = 10 V) is considered as the inner parent metal (target, a) while cesium (Cs, W_{Cs} = 3.54 V, ϕ_{Cs} = 1.95 V), Barium (Ba, ϕ_{Ba} = 2.52 V, W_{Ba} = 6.16 V), and Lithium (Li, ϕ_{Li} = 2.93 V, W_{Li} = 7.67 V) are considered as three independent (for 3 sets of parametric evaluation) coating materials (substrate, b). Other parameters used for computations are as follows: e_h = 0.2 V, d=5a_o and a_o = 600 nm; these values are physically plausible with real systems.[18–20] The effect of an individual parameter on the emission current has been evaluated by varying it over a wide range and keeping other factors the same. Using the analytical framework, the emission flux of electrons (I_{AB}), relative enhancement in emission current (I_{AB}/I_A) and the effective work function ($\phi_{virtual}$) of the coated surface has been evaluated and illustrated graphically as a function of coating thickness (s), surface temperature (T), base work function (ϕ_A) and width of the interface region (d). Note that, the width of the interface region (d) characterize the mutual interatomic interaction between the parent and coating material surfaces which eventually influences the electron emission flux through efficient tuning of the effective material work function. Since half width of the interface region ($d/2$) should not exceed the coating width (s), we can safely assume that: $d \equiv 2s$ for $s \leq d/2$ and $d \equiv d$ for $s > d/2$; this simply means the occurrence of high transition field in earlier case (thin coating) and consequently may lead to higher emission flux.

The effect of the thickness of the coating material on the emission flux (I_{AB}), current enhancement (I_{AB}/I_A) and virtual work function ($\phi_{virtual}$) have been illustrated in the set of Fig. 2. The current associated with electron emission from the coating surface (I_{AB}, Fig. 2a) is noticed to acquire a minimum around $s = d/2 \sim 2.5a_o$ while it increases around this minimum in s horizon namely in the region $s > 2.5a_o$ and $a_o \leq s \leq 2.5a_o$. In earlier case ($s > 2.5a_o$), this behavior can be understood in terms of increasing electron population within the coated sheet, while in the latter case ($a_o \leq s \leq 2.5a_o$) the nature may be attributed to the high electric field in the interface region. This high transition field within interface region effectively enhances the tunneling coefficient and hence diffusion flux of electrons from base material to the top layer coating sheet. Thus the electron population available for the emission within coating sheet is enhanced. In addition, the emission flux is observed to saturate at finite value with increasing coating thickness s. The Schottky effect is noticed to be much less pronounced[9] for the present set of parameters considered herein. The emission current is found to increase with increasing temperature which may be attributed to the increase in high energy electron population in the energy distribution tail. The suitable coating over the metal base may efficiently enhance the emission flux; this fact has been illustrated in Fig. 2b where the emission flux is found to enhance by more than three orders of magnitude. The enhancement in the flux due to surface coating acclaims a notion of flexibility to tune the emission current via suitable choice of the coating materials and its thickness. Using the estimates of the outcoming flux from the coating surface one may evaluate the effective work function of the composite system by comparing it with the thermionic emission flux associated with typical RD law (i.e. $\sim A_0T^2 exp(-\phi_{virtual}/k_BT)$); this virtual work function ($\phi_{virtual}$) has been illustrated as a function of coating thickness, in Fig. 2c. It is noticed that the adequate coating of the substrate over base metal efficiently reduces the work function ($\phi_{virtual}$); for instance Ag work function reduces to ~3.4 V due to Cs coating (Fig. 2c). The behaviour of $\phi_{virtual}$ with s is a consequence of emission current dependence on coating thickness (s).

The dependence of the emission flux (I_{AB}), current enhancement (I_{AB}/I_A) and virtual work function ($\phi_{virtual}$) on the operating temperature (T) in reference to the different coating substrates (Cs, Ba, *and* Li) for two prominently different choices of coating thickness *viz.* $s = a_o$ and $s = 10a_o$ are illustrated in the set of Fig. 3. The emission current (I_{AB}) increases with increase in the operating surface

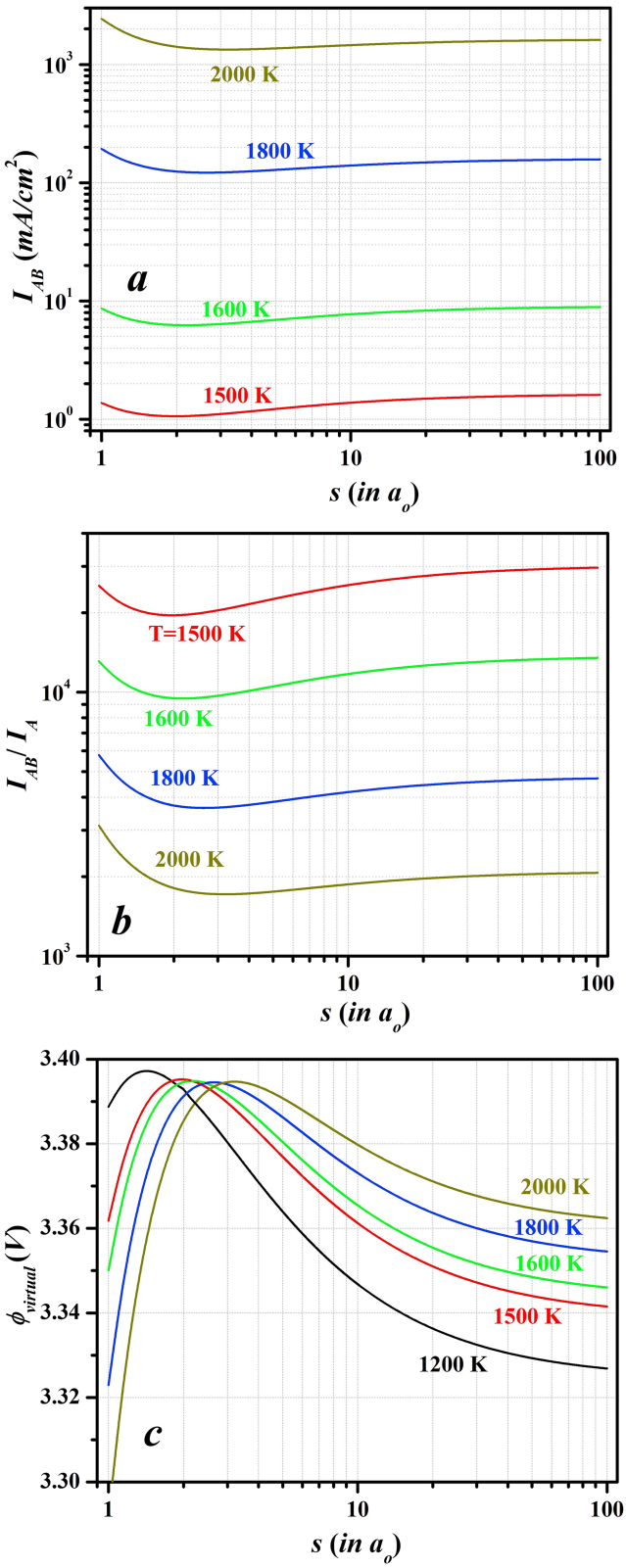

FIG. 2. Emission current (I_{AB}, 2a), current enhancement due to coating (I_{AB}/I_A, 2b) and virtual work function ($\phi_{virtual}$, 2c) as a function of width of the coating layer operating at different temperatures (T). The curves correspond to cesium (Cs) coating on parent silver (Ag) target with ϕ_{Ag} =4.5 V, W_{Ag} =10 V, ϕ_{Cs} =1.95 V, W_{Cs} =3.54 V, e_h =0.2 V and d=5a_o.

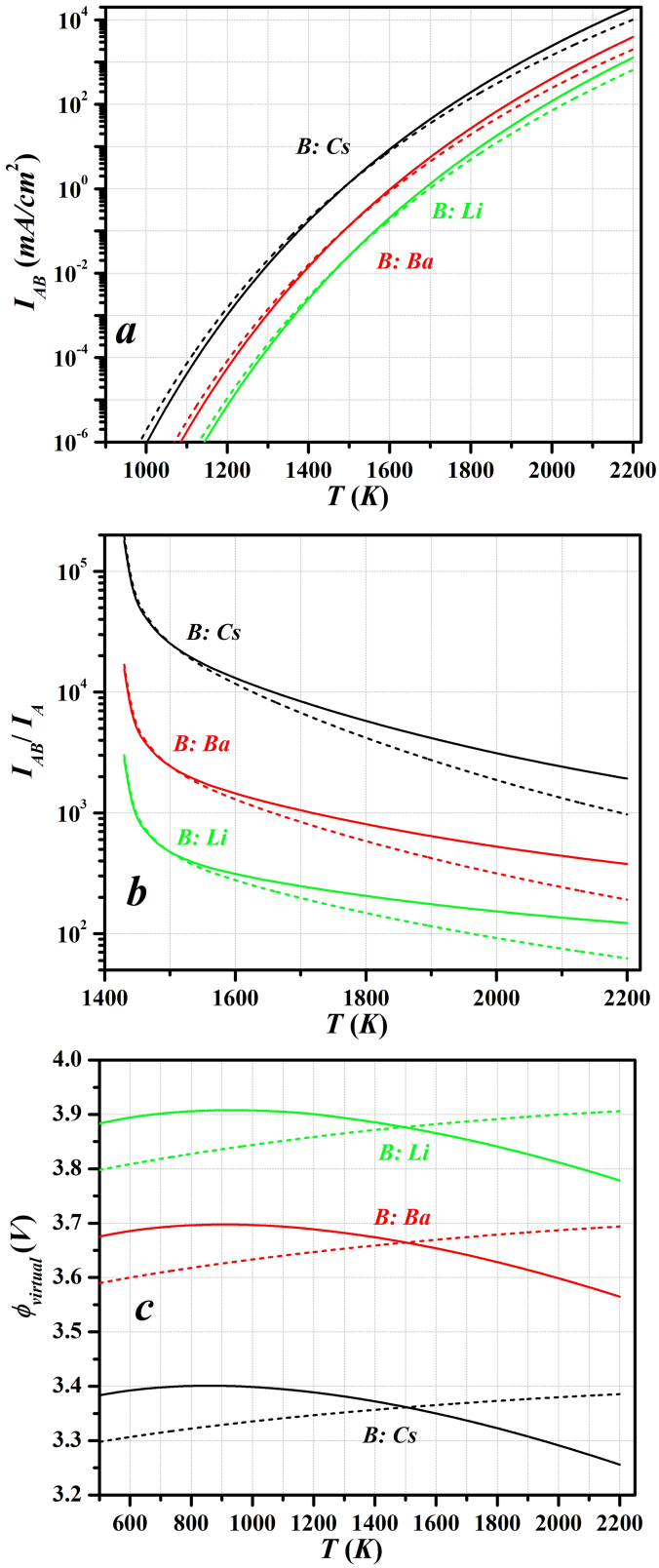

FIG. 3. Emission current (I_{AB}, 3a), current enhancement due to coating (I_{AB}/I_A, 3b) and virtual work function ($\phi_{virtual}$, 3c) as a function of the operating temperatures (T) for different coating materials. The curves correspond to parent silver (Ag) target (ϕ_{Ag} = 4.5 V, W_{Ag} = 10 V), coated with Cs (ϕ_{Cs} = 1.95 V, W_{Cs} = 3.54 V), Ba (ϕ_{Ba} = 2.52 V, W_{Ba} = 6.16 V), Li (ϕ_{Li} = 2.93 V, W_{Li} = 7.67 V), e_h = 0.2 V and d=5a_o; the solid and broken lines refer to the coating width s=a_o and s=10a_o, respectively.

temperature (Fig. 3a); this behaviour can be understood in terms of the enhanced electron population in the distribution function available for emission inside the composite coated surface. The emission flux associated with different coating substrates may be attributed to their respective work function; for instance the electron emission flux is noticed to relatively decrease with *Cs, Ba and Li* coating in reference to respective increase in their work function. We observe that the electron emission from the thinner coating ($s = a_o$, monoatomic layer) is pronounced at large operating temperature while a thick coating ($s = 10a_o$) infers nearly the bulk features, and is more effective at smaller temperature. This nature may be ascribed to the strong electric field tunneling associated with the interface region for monolayer ($s = a_o$) coating which is additionally aided with the availability of large population density of high energy electrons for emission at higher surface temperature (according to distribution function). For larger thickness ($s = 10a_o$) the contribution of the field emission decreases and thus the current is smaller at higher temperature in this case. At smaller temperature (~1400 K) the emission current is dominated by the electron population density available for emission which is larger in case of $s = 10a_o$ than that of monolayer coating. The two cases (namely $s = 10a_o$ and $s = a_o$) thus meet

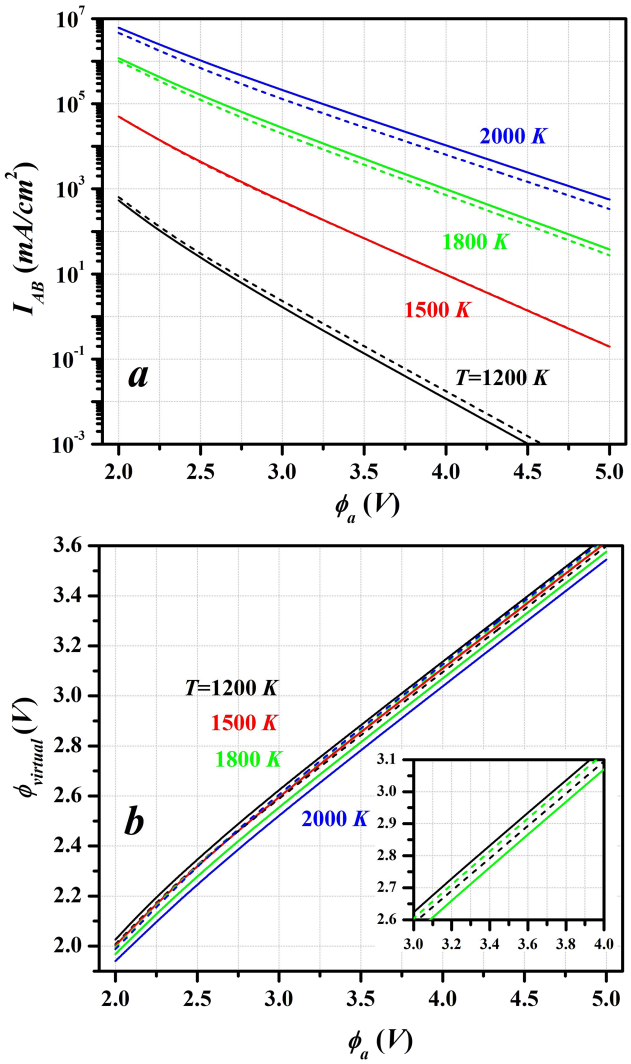

FIG. 4. Emission current (I_{AB}, 4a) and virtual work function ($\phi_{virtual}$, 4b) as a function of work function of the base material (ϕ_a) operating at different temperatures (T). The curves correspond to cesium (Cs) coating (ϕ_{Cs} = 1.95 V, W_{Cs} = 3.54 V), W_a = 10 V, e_h = 0.2 V, and d=5a_o; the solid and broken lines refer to the coating width s=a_o and s=10a_o, respectively. Inset in (b) shows enlarged representation in ϕ_a range of 3.0 – 4.0V.

around surface temperature ~1500 K, which apparently infers the same value of virtual work function. The consequent temperature dependence of the current enhancement factor (I_{AB}/I_A) and virtual work function are depicted in Fig. 3b and Fig. 3c, respectively; the behaviour may be accredited to the varying work function of the coating materials and temperature dependence of the emission current (I_{AB}, Fig. 3a).

The effect of the varying work function of the parent (target) material (ϕ_a) for a particular coating type (*Cs* coated surface) operating at various temperatures for two extreme choices i.e. $s = a_o$ and $s = 10a_o$, on the emission current (I_{AB}) and virtual work function ($\phi_{virtual}$) have been illustrated in Fig. 4. With increase in ϕ_a, the barrier height for electron diffusion through interface region III increases, resulting in reduction in effective emission flux. For a particular ϕ_a value, below 1500K, emission current I_{AB} is found to be higher for the thicker coating, while above 1500K, I_{AB} enhances with reduction in coating thickness (see the broken lines location with respect to respective solid lines for T=1200K and 1800K, Fig. 4a). The change in thickness dependence of current is more discretely visible in Fig. 4b inset. The efficient current in the case of thinner coating at high temperature is also visualized here, as discussed before in case of Fig. 3a. The estimate of the virtual work function corresponding to this figure (Fig. 4a) has been illustrated in Fig. 4b which is primarily a consequence of the equivalence between net emission current (via present formulation) with RD relation. The figure also indicates that the effective lowering of the work function due to coating is more pronounced for higher ϕ_a; this may be understood in terms of the higher electrostatic potential (field) across the interface region causing large emission current. A significant enhancement in the emission current is noticed when both ϕ_a and ϕ_b are low but $(\phi_a - \phi_b)$ is substantially large, as evident in the Fig. 5. From the slope of the I_{AB} vs ϕ_a curves in Fig. 5, we understand that lower is the operational temperature stronger is the dependence of I_{AB} on ϕ_a. The dependence of the emission flux and corresponding virtual work function on the width of the transition layer d (inherently inferring the field strength) with respect to Cs coated surfaces has been depicted in the set of Fig. 6. The increase in the emission current with decreasing d may be explained on the basis of efficient electron flux associated with strong electric field across the interface region; this behaviour has been displayed in Fig. 6a. As illustrated in Fig. 6b, the virtual work function associated with coated surface is noticed to decrease significantly with decrease in the width of the interface region (d). This nature is again a consequence of enhancement in emission current scaling with RD emission law. It should be mentioned that though the effect has been illustrated for a particular combination of the parent and coating materials, the conceptual basis is applicable to any general case.

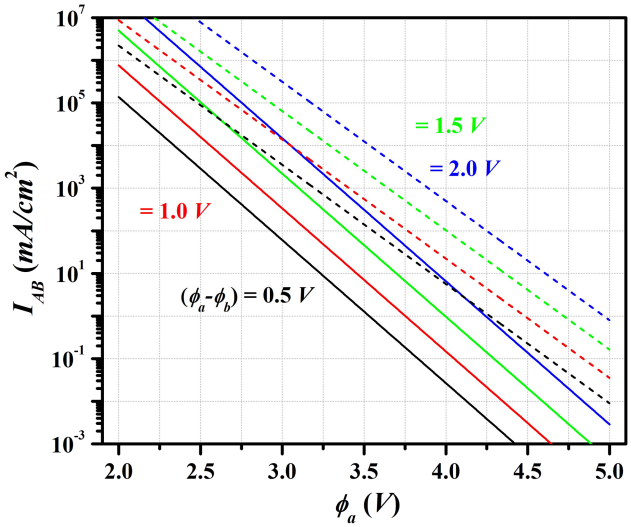

FIG. 5. Emission current (I_{AB}) as a function of parent target material work function (ϕ_a) for different values of ($\phi_a - \phi_b \equiv 2V_0$). The curves correspond to W_a = 10 V, W_b = 7 V, e_h = 0.2 V, s=10a_o and d=5a_o; the solid and broken lines refer to the surface temperature T=1500 K and T=1800 K respectively.

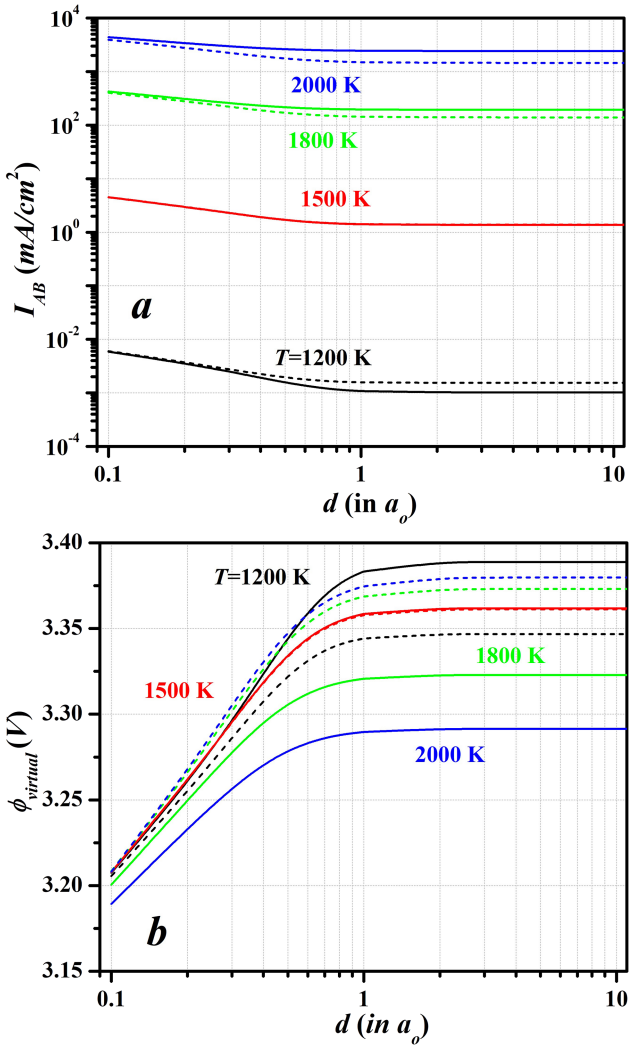

FIG. 6. Emission current (I_{AB}, 6a) and virtual work function ($\phi_{virtual}$, 6b) as a function of interface width (d) for different operating temperatures (T). The curves correspond to cesium (Cs) (ϕ_{Cs} = 1.95 V, W_{Cs} = 3.54 V) coated silver (Ag) target (ϕ_{Ag} = 4.5 V, W_{Ag} = 10 V), e_h = 0.2 V, and d=5a_o; the solid and broken lines refer to the coating width s=a_o and s=10a_o, respectively.

IV. SUMMARY AND REMARKS

In summary, the electron emission from the coating surfaces operating at a finite temperature has been investigated; the effect of the coating substrates in terms of different materials and thickness has been rigorously examined. The surface coating eventually creates a high electric (potential) field interface with parent metal target which ultimately enhances the electron emission flux (or current). In order to analyze the emission from a coated metal target, a formalism based on the Fowler's treatment of the electron emission along with adequate energy dispersion for the parent material (parabolic) and coating materials (thickness dependent non-parabolic) in estimating the total density of states for the Fermionic electrons (FD statistics) has been established. The present formulation holds good for any metal/semiconductor combination. The electron emission flux from the coating surfaces has been derived as a function of material specifications and coating thickness; the conceptual basis has quantitatively been appreciated through numerical calculations within specific parametric regime. As a significant feature, the electron emission flux from the coated surfaces is found to be sensitive to not only the materials, but also the coating thickness. Our results in fact suggest that coating thickness can be utilized suitably to tune the electron emission at a desired operational temperature.

While some surface coatings are considered highly reactive, and surface nano-structuring is being considered as a more suitable route to tune electron emission,[24] simple geometric modulation through coating thickness seems to provide an easy and additional means to control emission current. The electron emission flux is more pronounced in high temperature regime (above 1500K) for the thin coating, while thicker coating result in more efficient emission at lower temperature. The analysis predicts fine tuning of the electron emission flux up to desired extent via adequate choice of physical parameters of the coating substrates and parent (base) material. The insight of the electron emission phenomenon, the formulation and flux (current) estimates in reference to the coating surfaces formulated in this analysis may be of practical implications in the fabrication of efficient/tunable field emitters and thin film devices.

ACKNOWLEDGMENTS

The work is performed under ELI-ALPS project (GINOP-2.3.6-15-2015-00001) which is supported by European Union and co-financed by European Regional Development fund.

[1] H. Zhang, J. Tang, J. Yuan, Y. Yamauchi, T. T. Suzuki, N. Shinya, K. Nakajima, and L.-C. Qin, "An ultra-bright and monochromatic electron point source made of a LaB6 nanowire," Nat. Nanotechnol. **11**, 273–279 (2016).
[2] G. Chen and Y. Song, "Field emission from lateral multiwalled carbon nanotube yarn emitters," Front. Mater. **3**, 1–6 (2016).
[3] Z. Zulkifli, S. Munisamy, M. Z. M. Yusop, and M. Tanemura, "Effect of surface morphology \non the field emission property of ZnO films," Phys. Status Solidi C **1352**, 1–4 (2014).
[4] S. Sridhar, L. Ge, C. S. Tiwary, A. C. Hart, S. Ozden, K. Kalaga, S. Lei, S. V. Sridhar, R. K. Sinha, H. Harsh, K. Kordas, P. M. Ajayan, and R. Vajtai, "Enhanced field emission properties from CNT arrays synthesized on inconel superalloy," ACS Appl. Mater. Interfaces **6**, 1986–1991 (2014).
[5] J. Jiang, J. Zhang, T. Feng, B. Jiang, Y. Wang, F. Zhang, L. Dai, X. Wang, X. Liu, and S. Zou, "Improved emission stability of HfC-coated carbon nanotubes field emitters," Solid State Commun. **135**, 390–393 (2005).
[6] P. Ruffieux, O. Gröning, M. Bielmann, and P. Gröning, "Hydrogen chemisorption on sp 2-bonded carbon: Influence of the local curvature and local electronic effects," Appl. Phys. A Mater. Sci. Process. **78**, 975–980 (2004).
[7] T. P. Kaloni, M. U. Kahaly, Y. C. Cheng, and U. Schwingenschlögl, "Mechanism of Si intercalation in defective graphene on SiC," J. Mater. Chem. **22**, 23340–23343 (2012).
[8] M. U. Kahaly and U. V. Waghmare, "Contrast in the electronic and magnetic properties of doped carbon and boron nitride nanotubes: A first-principles study," J. Phys. Chem. C **112**, 3464–3472 (2008).
[9] M. U. Kahaly, "Defect states in carbon nanotubes and related band structure engineering: A first-principles study," J. Appl. Phys. **105**(2), 024312 (2009).
[10] H. Yuan, S. Chang, I. Bargatin, N. C. Wang, D. C. Riley, H. Wang, J. W. Schwede, J. Provine, E. Pop, Z. X. Shen, P. A. Pianetta, N. A. Melosh, and R. T. Howe, "Engineering ultra-low work function of graphene," Nano Lett. **15**, 6475–6480 (2015).
[11] C. M. Collins, R. J. Parmee, W. I. Milne, and M. T. Cole, "High performance field emitters," Adv. Sci. **3**, 1–8 (2015).
[12] K. A. A. Khalid, T. J. Leong, and K. Mohamed, "Review on thermionic energy converters," IEEE Trans. Electron Devices **63**, 2231–2241 (2016).
[13] J. Deng, B. Zhang, N. Yao, and L. Fang, "Field emission from metal-coated nano-crystalline graphitic films," IVNC IFES 2006-Tech. Dig. - l9th Int. Vac. Nanoelectron. Conf. 50th Int. F. Emiss. Symp. 536, 283–284 (2006).
[14] F. Seitz, *The Modern Theory of Solids* (McGraw Hill, New York, 1940).
[15] R. H. Fowler, *Statistical Mechanics: Theory of the Properties of Matter in Equilibrium* (Cambridge University Press, Cambridge, 1980).
[16] S. Agarwal, S. Misra, S. K. Mishra, and M. S. Sodha, "Three region model and quantum enhancement of thermionic and photoelectric electron emission from negatively charged metallic surfaces," Can. J. Phys. **90**, 265–275 (2012).
[17] S. K. Mishra, M. S. Sodha, and S. Misra, "Quantum effects in electron emission from and accretion on negatively charged spherical particles in a complex plasma," Phys. Plasmas **19**, 1–11 (2012).
[18] A. K. Ghatak and S. Lokanathan, *Quantum Mechanics: Theory & Applications*, (Kluwer Academic Publishers: London, 2004).
[19] M. S. Sodha, *Kinetics of complex plasmas* (Springer, New Delhi, 2014).
[20] Y. S. Ang and L. K. Ang, "Current-temperature scaling for a Schottky interface with nonparabolic energy dispersion," Phys. Rev. Appl. **6**, 1–10 (2016).
[21] S. Misra, S. K. Mishra, and M. S. Sodha, "Photoelectric sheath formation around small spherical objects in space," Phys. Plasmas **22**, 043705 (2015).
[22] S. Misra, M. Upadhyay Kahaly, and S. K. Mishra, "Thermionic emission from monolayer graphene, sheath formation and its feasibility towards thermionic converters," J. Appl. Phys. **121**, 065102 (2017).
[23] M. Upadhyay Kahaly, S. Misra, and S. K. Mishra, "Photo-assisted electron emission from illuminated monolayer graphene," J. Appl. Phys. **121**, 205110 (2017).
[24] K. T. Narasimha, C. Ge, J. D. Fabbri, W. Clay, B. A. Tkachenko, A. A. Fokin, P. R. Schreiner, J. E. Dahl, R. M. K. Carlson, Z. X. Shen, and N. A. Melosh, "Ultralow effective work function surfaces using diamondoid monolayers," Nat. Nanotechnol. **11**, 267–272 (2015).